JOURNAL OF MATERIALS SCIENCE 21 (1986) 692–704

# A fractographic study of hydrogen-assisted cracking and liquid-metal embrittlement in nickel

S. P. LYNCH
*Aeronautical Research Laboratories, Defence Science and Technology Organisation, Department of Defence, Melbourne, Australia*

Metallographic and fractographic studies of crack growth in nickel polycrystals and single crystals in a number of environments are described. "Brittle" intercrystalline and transcrystalline cleavage-like fractures were observed for specimens tested in liquid mercury, liquid lithium, liquid sodium, gaseous hydrogen, and for hydrogen-charged specimens tested in air. "Brittle" fractures were associated with considerable slip, and dimples/tear ridges were observed on fracture surfaces, suggesting that crack growth occurred by localized plastic flow. There were remarkable similarities between adsorption-induced liquid-metal embrittlement and hydrogen-assisted cracking which, along with other observations, suggested that adsorbed hydrogen at crack tips was responsible for hydrogen-assisted cracking. It is concluded that adsorbed atoms weaken interatomic bonds at crack tips thereby facilitating the nucleation of dislocations and promoting crack growth by localized plastic flow.

## 1. Introduction

The fracture resistance of nickel and its alloys is generally decreased by the presence of hydrogen. Furthermore, changes in fracture mode from ductile dimpled fractures in inert environments to brittle intercrystalline or transcrystalline cleavage-like fractures in hydrogen environments are often observed [1–6]. The material and testing conditions, e.g. microstructure, hydrogen pressure (or content), temperature, and strain rate determine the degree of embrittlement and the fracture mode.

Plastic flow in nickel can also be affected by the presence of hydrogen – serrated yielding and hardening have been observed in some circumstances [7–11] while softening has been observed in others [12, 13]. In other words, dislocation motion can be either inhibited or promoted by the presence of hydrogen depending on the experimental conditions; increased dislocation activity due to hydrogen has been directly observed in thin foils using high-voltage electron microscopy [13]. However, hydrogen-charged and uncharged specimens generally show similar dislocation arrangements after deformation [14 15].

Mechanisms of hydrogen-assisted cracking (HAC) are not well understood and a number of conflicting proposals have been made. Some workers have suggested that HAC is associated with the effects of dissolved hydrogen on slip – arguing that solute hydrogen either inhibits slip thereby favouring "decohesion" at crack tips [16] or, conversely, facilitates slip thereby promoting cracking by localized plasticity at crack tips [2, 12, 13]. Other workers have suggested that HAC is due to weakening of interatomic bonds at crack tips by adsorbed hydrogen. Such an effect could facilitate either decohesion at crack tips [3] or nucleation of dislocations from crack tips [4], the latter promoting fracture by localized plastic flow.

Liquid-metal embrittlement (LME) is less complex than HAC since embrittling atoms do not usually diffuse into the solid and, hence, embrittlement can generally be attributed to the presence of adsorbed liquid-metal atoms at crack tips [17, 18]. LME of nickel has received less attention than HAC but embrittlement by mercury [4], lithium [19], and cadmium–caesium [20] has been reported. Preliminary studies by the present author [4] showed that the characteristics of fracture in nickel single crystals in liquid mercury were similar to those produced by fracture in gaseous hydrogen suggesting that mechanisms of LME and HAC may be the same.

In the present paper, further studies of HAC and LME have been made to substantiate and extend the preliminary work. Polycrystalline and single crystal specimens have been tested in inert environments (with and without prior hydrogen charging), gaseous hydrogen, liquid mercury, and liquid alkali metals. These metals can readily be removed from fracture surfaces so that detailed fractographic observations can be made. Mechanisms of HAC and LME are discussed in the light of these results and of recent work by others.

## 2. Experimental details

### 2.1. Material and heat treatment

Most specimens were cut from 2.5 mm thick sheets of nickel 200 ($\simeq$99.5 Ni, 0.22 Fe, 0.19 Mn, 0.08 Cu, 0.04 C, 0.01 Si, 0.01 S, wt %). Polycrystalline specimens were annealed at 900° C for 1 h, and then slowly cooled, producing a grain size $\simeq 100\,\mu$m. "Single-crystal" specimens with a wide variety of orientations



0022–2461/86 $03.00 + .12 

were prepared by (a) annealing sheet at 1400° C in vacuum for 24 h producing grain sizes up to ≃ 20 mm, (b) cutting specimens from the sheet such that a large grain was at the centre of specimens, and (c) cutting a central notch on one edge of specimens so that cracks initiated and grew across the central grain.

Some polycrystalline and single-crystal specimens were hydrogen-charged by re-annealing at 1000° C in ≃ 100 kPa hydrogen gas for 1 h and then quenching into water at 0° C; this procedure reportedly [1] results in a solute hydrogen concentration of ≃ 0.045 at %.

Several single crystal specimens of high-purity (> 99.99%) nickel, with a near-⟨1 1 1⟩ specimen axis, from a study of HAC by Kamdar [3] were re-examined; some of his specimens were also tested in liquid mercury in the present study.

### 2.2. Environments

Specimens were tested in (a) dry argon, (b) dry hydrogen (≃ 99.995% purity) at ≃ 101 kPa pressure, (c) laboratory air, (d) liquid mercury (all at ≃ 25° C), (e) liquid lithium at ≃ 210° C, (f) liquid sodium at ≃ 120° C, (g) liquid potassium at ≃ 75° C, (h) liquid rubidium at ≃ 50° C, and (i) liquid caesium at ≃ 40° C. The test temperatures in the alkali metals are within ≃ 30° C of their melting temperatures. Tests in the liquid alkali metals were carried out at AERE, Harwell using their inert atmosphere handling and testing facilities [21].

### 2.3. Testing

Specimens were tested in tension at a crosshead-displacement rate of 0.033 mm $sec^{-1}$ or in cantilever bending at displacement rates of ≃ 5° $sec^{-1}$ and ≃ 0.0006° $sec^{-1}$. Tensile specimens, with a 3 mm × 2.5 mm cross-section and a 1 mm deep notch, were used for tests in the liquid alkali metals. Kamdar's single crystal specimens, with a 2 mm × 1.4 mm cross-section and a 0.6 mm deep notch were also tested in tension. Cantilever-bend specimens, with a 7 mm × 2.5 mm cross-section, a 1 mm deep notch, and a 1 mm deep fatigue pre-crack, were used for other tests.

### 2.4. Examination of specimens

Deformation associated with cracking was observed on the chemically polished side surfaces of specimens. Fracture surfaces were examined by scanning electron microscopy (SEM) and transmission electron microscopy (TEM) of secondary-carbon replicas. Prior to examination, mercury was evaporated from fracture surfaces at 100° C in vacuum and the alkali metals were dissolved in methanol; plastic replicas were also stripped from fracture surfaces to remove any remaining loose deposits.

Orientations of fracture planes were determined in two ways: (i) from the angle between fracture planes and single-crystal specimen axes which were established from Laue X-ray back-reflection patterns, and (ii) from the angles between slip traces on fracture surfaces; the fracture surfaces were sometimes lightly chemically polished and then deformed so that four sets of slip lines were clearly visible.

TABLE I Approximate proportions of fracture modes observed in different environments

| | Li | Na | Hg | $H_2$ | H |
|---|---|---|---|---|---|
| % Intercrystalline | 98 | 10 | 30 | 5 | 25 |
| % Cleavage-like | 2 | 40 | 45 | 75 | 15 |
| % Dimpled | – | 50 | 25 | 20 | 60 |

## 3. Results

### 3.1. Fracture in polycrystalline specimens

In air or argon environments, ductile transcrystalline fractures with large, deep dimples on fracture surfaces were observed. Small inclusions were often observed within the dimples and the sides of dimples were covered with slip markings. Ductile fracture was also observed after rapid fracture in hydrogen-charged specimens, and specimens tested in a caesium, rubidium, and potassium (Fig. 1a).

Embrittlement was observed for (i) slow crack growth ($6 \times 10^{-5}$ mm $sec^{-1}$) in hydrogen-charged specimens, (ii) crack growth in hydrogen gas (at velocities as high as ≃ 1 mm $sec^{-1}$), and (iii) crack growth in liquid lithium, liquid sodium, and liquid mercury. Embrittlement in lithium was severe but for the other environments there was considerable, macroscopic plasticity associated with fracture. Fracture surfaces exhibited "brittle" intercrystalline regions, transcrystalline cleavage-like regions, and areas of large dimples (Figs. 1b to f); the proportion of each depended on the environment (Table I).

However, the appearance of both intercrystalline and cleavage-like fractures were similar in all cases. Intercrystalline fractures were generally covered with slip traces, and sometimes by tear ridges or shallow dimples (Figs. 2a to d). Cleavage-like fractures were similar to those observed in single crystals, described in detail below.

### 3.2. Fracture of single crystals in hydrogen gas and mercury

#### *3.2.1. General observations*

Rapid crack growth (≃ 1 mm $sec^{-1}$) in hydrogen and mercury environments resulted in a similar degree of embrittlement and remarkably similar fracture-surface characteristics. For a given crack-opening displacement, increments of crack growth were about three times larger in hydrogen and mercury environments than in inert environments. Crack-tip profiles produced by fracture in mercury and hydrogen were also similar and there was much less blunting at crack tips in hydrogen and mercury than in inert environments (Fig. 3).

#### *3.2.2. Deformation associated with fracture*

The extent and distribution of slip around cracks was similar for mercury and hydrogen environments with slip occurring particularly on planes intersecting the crack-tip region. This was most clearly evident around fatigue precracks (Figs. 4a and b) since slip associated with overload fracture in mercury and hydrogen was very intense (Fig. 4c) with lateral contractions of the specimen side of up to 50% of the specimen thickness. Nevertheless, this slip was less extensive and more

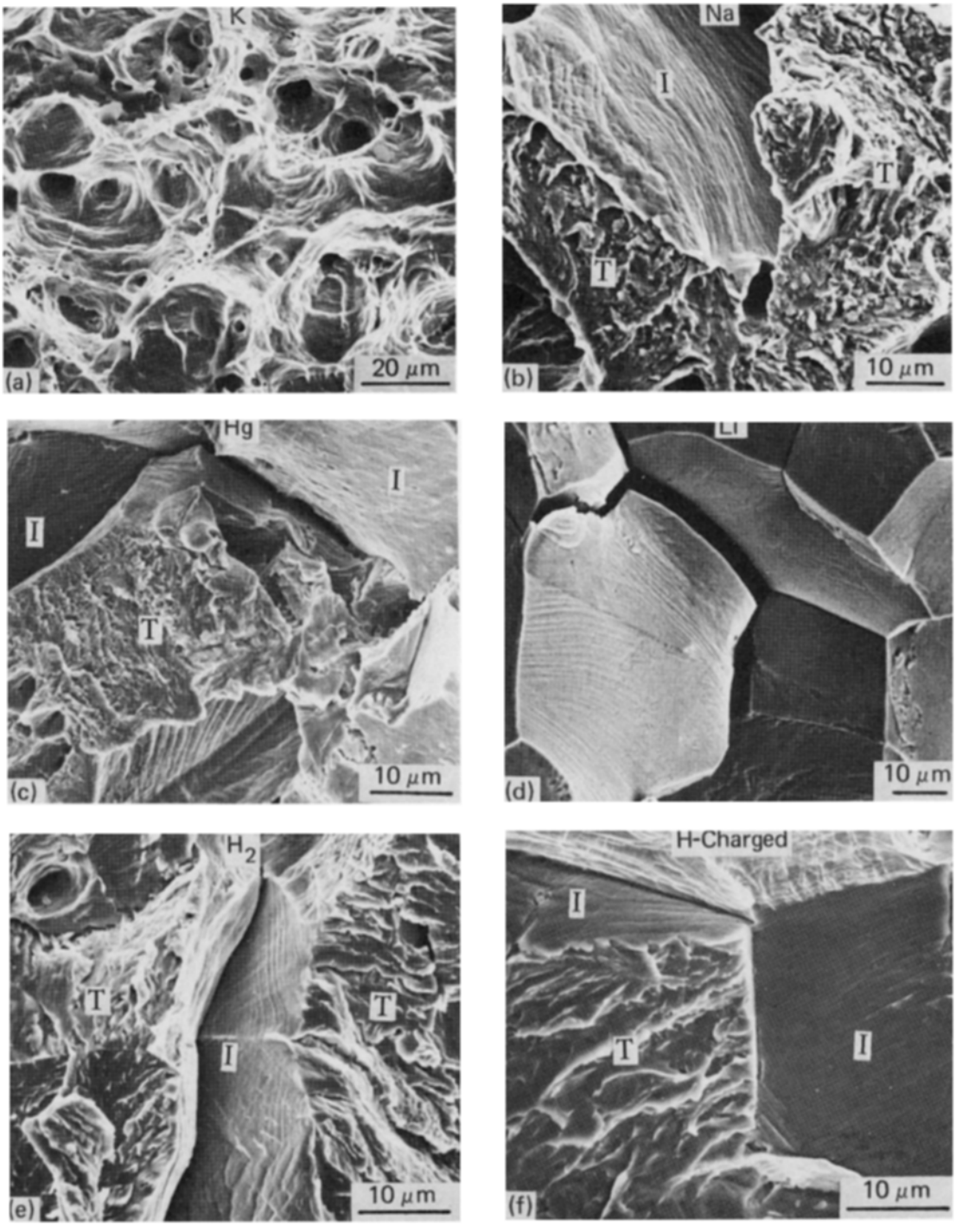


*Figure 1* SEM of fracture surfaces for nickel polycrystals cracked in (a) liquid potassium, (b) liquid sodium, (c) liquid mercury, (d) liquid lithium, (e) gaseous hydrogen, and (f) air at slow strain rates after hydrogen-charging. A ductile dimpled fracture is produced in potassium whereas "brittle" intercrystalline (I) and transcrystalline (T) cleavage-like fractures are produced in the other environments.

localized around crack tips than slip associated with crack growth in inert environments.

### 3.2.3. Appearance of fracture surfaces

The fracture-surface appearance depended somewhat on the orientation of specimens but, for a given orientation, fractures produced in mercury and hydrogen were identical. This was dramatically illustrated by cracking the same specimen first in mercury and then, after evaporating the mercury from the crack, in hydrogen. The crack was generally closed slightly after evaporating the mercury to produce a striation on the fracture surface since otherwise it was difficult to distinguish between the regions cracked in mercury and hydrogen (Figs. 5 and 6). Fracture surfaces of specimens cracked in mercury and then, after evaporating the mercury, in air, showed an abrupt change from a brittle to a ductile fracture mode. Thus, there was no doubt that mercury was completely removed by the evaporation procedure.

Fracture surfaces exhibited river lines, serrated steps, tear ridges, slip lines, secondary cracks, and dimples. The appearance of opposite fracture surfaces often differed significantly, with one surface exhibiting more secondary cracking and slip lines than the other (Fig. 7). Since the slip lines on one fracture surface

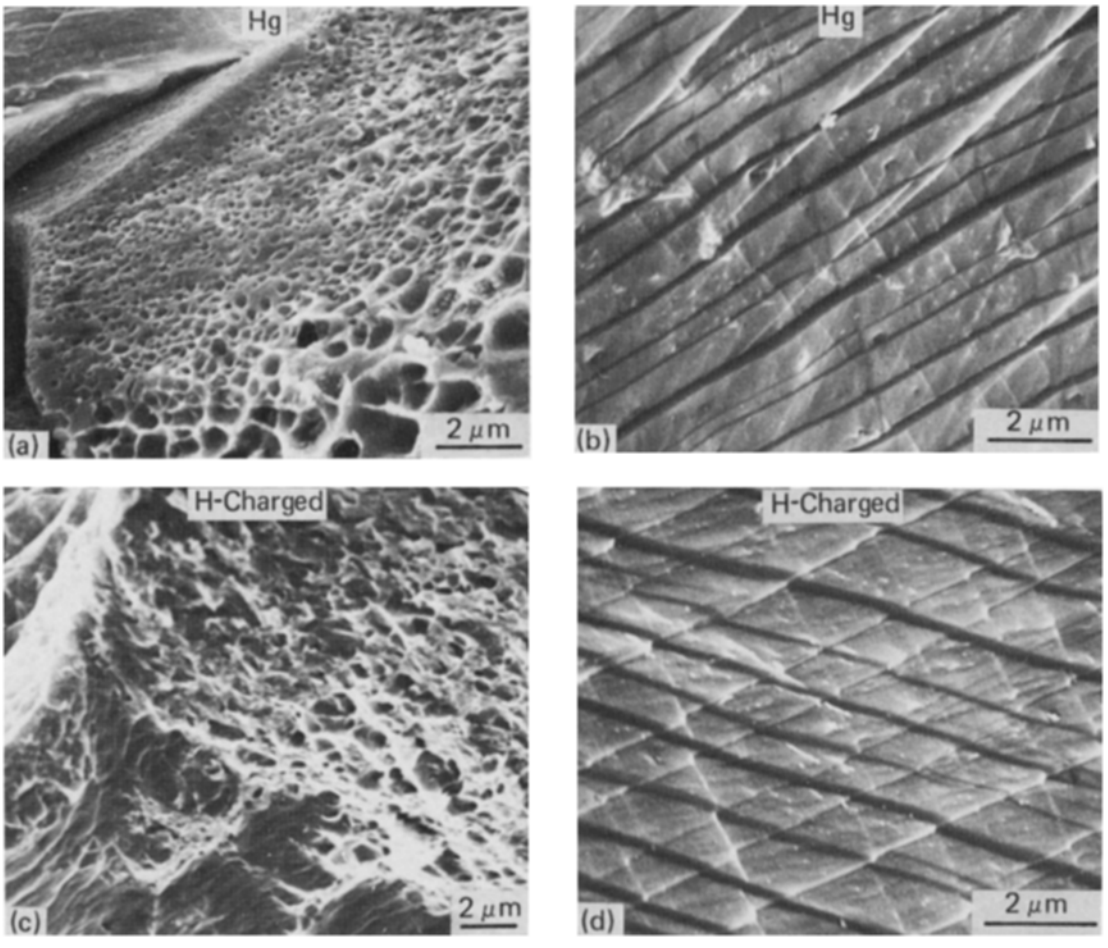


*Figure 2* SEM of intercrystalline fracture surfaces produced by crack growth in (a and b) liquid mercury, and (c and d) hydrogen-charged specimen, at a higher magnification showing dimpled facets (a and c) and relatively smooth facets except for slip lines (b and d).

were not generally matched by slip lines on the other surface, they are not crack-arrest markings but are probably produced by slip behind the crack tip.

Isolated dimples on fracture surfaces were quite large and were associated with voids nucleated from cracked inclusions (Fig. 7). The three-pronged tear ridges, which "point" in the direction of crack growth, probably result when cracks intersect voids since particles and dimples were sometimes visible just in front of tear ridges (Fig. 8)*. There were also many, small, shallow dimples which were revealed by TEM but not by SEM (Fig. 9).

Examination of specimens of high-purity nickel cracked in hydrogen gas by Kamdar [3] and comparison of these specimens with high-purity specimens cracked in mercury in the present work also showed that the characteristics of fracture in mercury and hydrogen were similar (Figs. 10, 11). These fracture surfaces were also similar to fracture surfaces in the 99.5% purity nickel described above except that large dimples were not observed in the purer material.

### 3.3. Crack growth in hydrogen-charged single crystals

Fracture surfaces of both hydrogen-charged and uncharged specimens exhibited stretched zones and

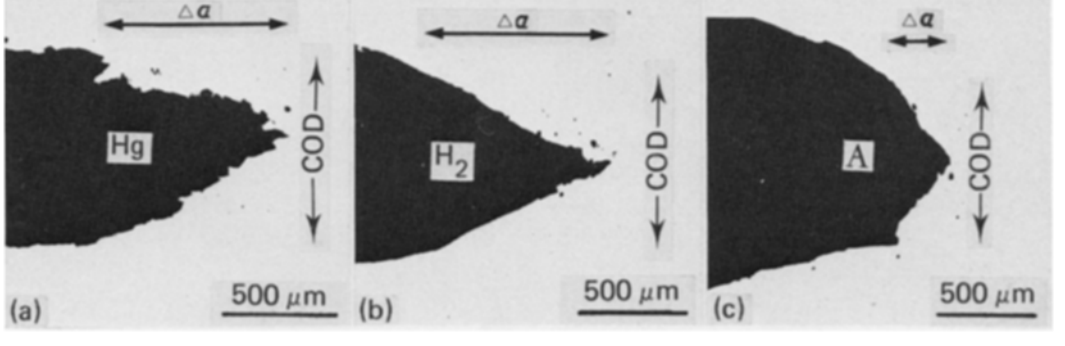


*Figure 3* Optical micrographs of sections through single crystal specimens fatigue precracked and then cracked in (a) mercury, (b) gaseous hydrogen, and (c) argon showing the extent of crack growth, $\Delta a$, for a given crack-opening displacement, COD.

*It has also been suggested [5] that the tear ridges are formed by necking of ligaments of material left behind the main crack front. However, it is not clear why such ligaments should be formed in essentially homogeneous single crystals.

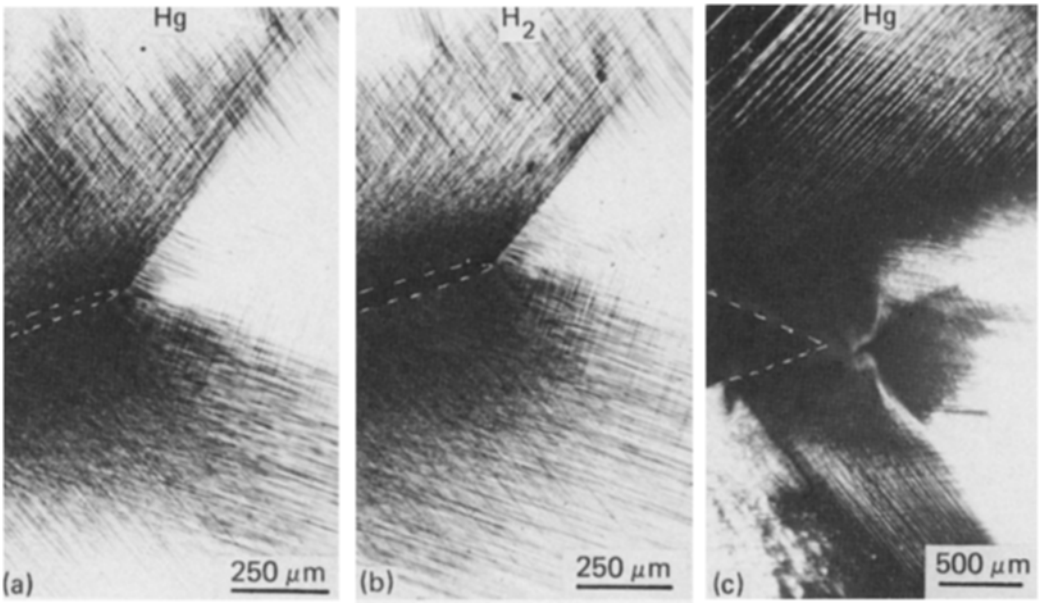


*Figure 4* Optical micrographs showing slip on the side surface of single crystal specimens (a) fatigue precracked in mercury, (b) fatigue precracked in gaseous hydrogen, and (c) cracked by increasing the COD in mercury.

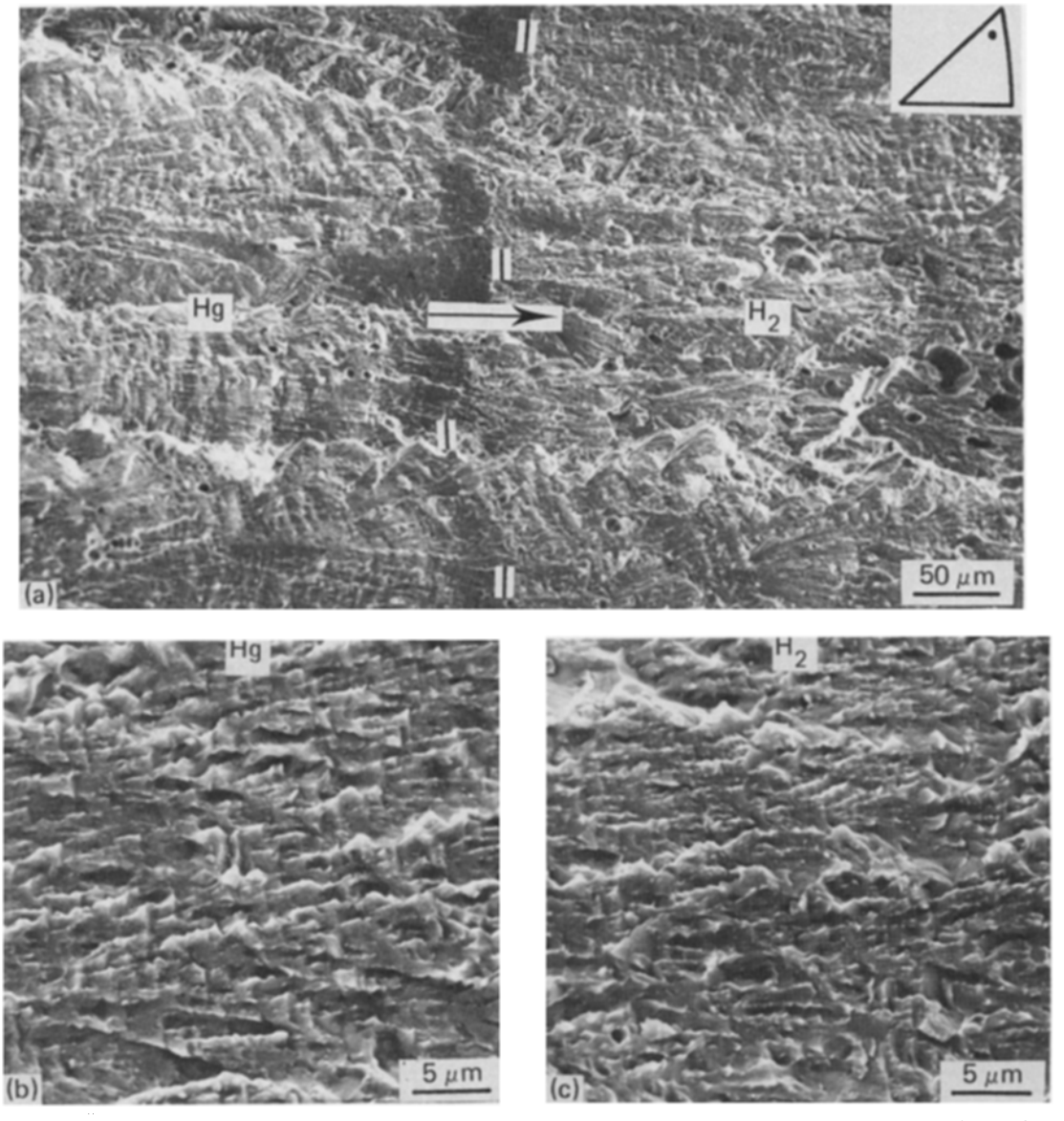


*Figure 5* (a) SEM of fracture surface of a near ⟨1 1 1⟩ single crystal produced by crack growth in mercury and then hydrogen (see text). (b and c) SEM of regions produced by fracture in mercury and hydrogen, respectively, at a higher magnification showing serrated steps, tear ridges, dimples, and slip lines.

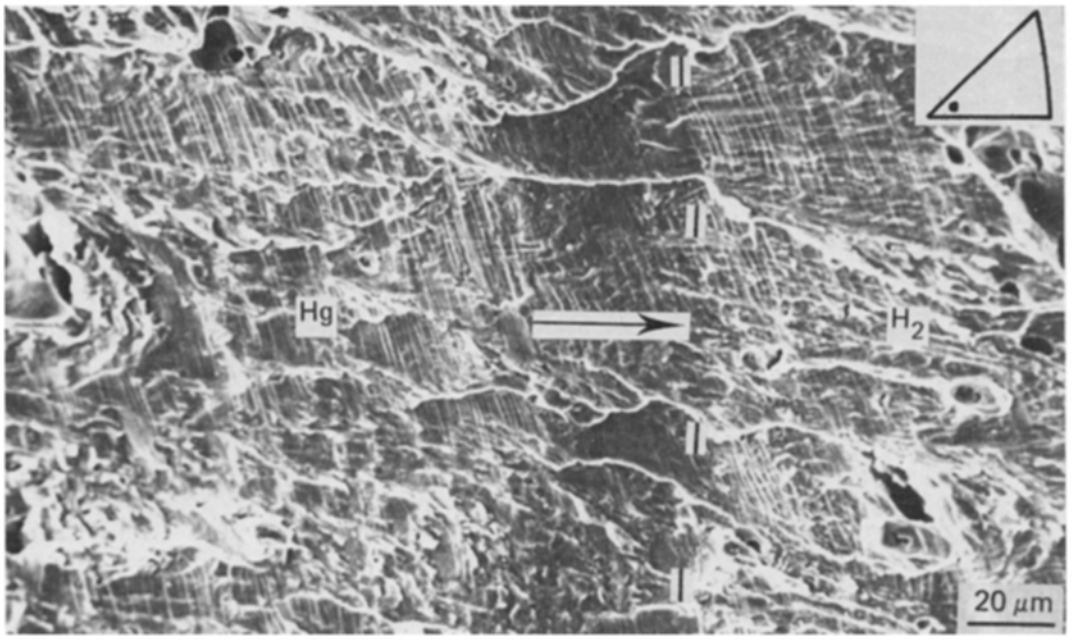


*Figure 6* SEM of fracture surface of a near ⟨1 0 0⟩ single crystal produced by crack growth in mercury and then hydrogen. The fracture-surface appearance differs somewhat from the near ⟨1 1 1⟩ orientation (see Fig. 5) but, as for the near ⟨1 1 1⟩ crystal, the appearance produced by crack growth in mercury and hydrogen is identical.

large dimples around the tips of fatigue precracks, i.e. there was no evidence of embrittlement (Fig. 12). (Specimens were hydrogen-charged prior to fatigue and there was also no effect of hydrogen-charging on the appearance and spacing of fatigue striations). However, brittle areas were observed around some large dimples further ahead of fatigue pre-cracks in hydrogen-charged specimens fractured slowly ($\simeq 6 \times 10^{-5}$ mm sec$^{-1}$) (Fig. 13). These brittle areas were similar to those produced in specimens cracked in gaseous hydrogen.

### 3.4. Orientation of "brittle" fracture planes

Laue X-ray back-reflection photographs from fracture surfaces showed only a few extremely diffuse spots confirming that strains beneath fracture surfaces were high. Orientations of fracture surfaces (on a macroscopic scale) were therefore determined from the angle between the specimen axis and the fracture plane, and from the angles between slip traces on fracture surfaces.

For specimens with a near-⟨1 0 0⟩ orientation, four sets of slip lines on fracture surfaces formed an

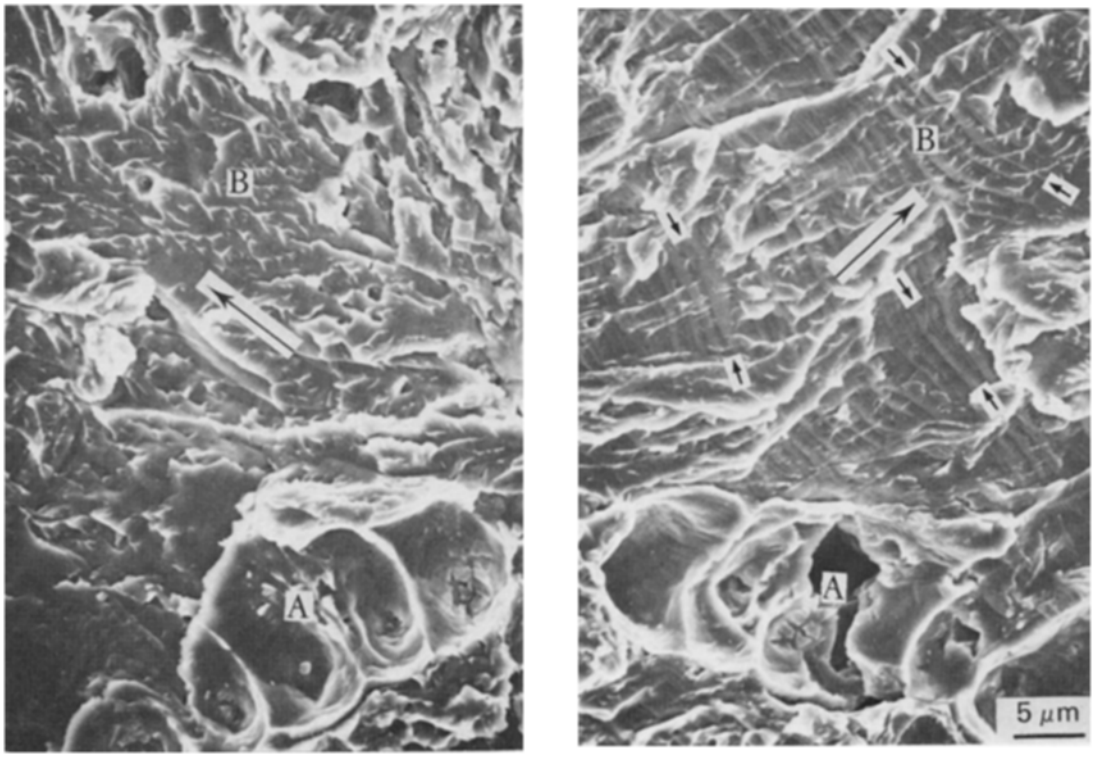


*Figure 7* SEM of mating halves of opposite fracture surfaces produced by crack growth in gaseous hydrogen (same specimen as in Fig. 6) showing dimples (A), tear ridges (B), and numerous slip lines (small arrows) on one fracture surface but not the other.

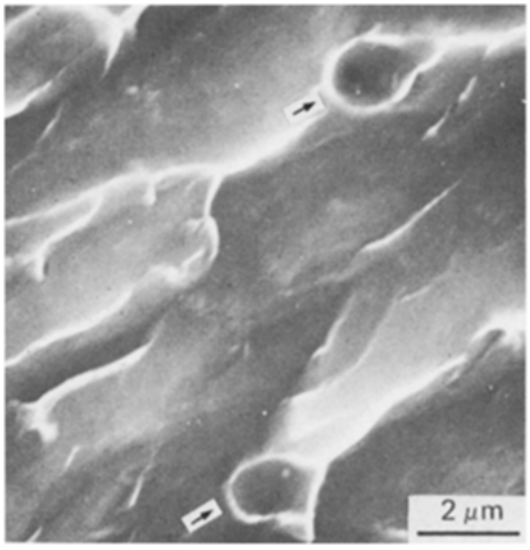


*Figure 8* SEM of fracture surface of nickel single crystal produced in hydrogen showing small dimples (arrowed) associated with tear ridges.

approximate orthogonal network showing that fracture planes were close to a {1 0 0} plane. Crack fronts were generally parallel to slip lines showing that crack growth occurred in ⟨1 1 0⟩ directions. Crack growth sometimes occurred in different ⟨1 1 0⟩ directions in adjacent regions so that crack fronts were at right angles to each other (Fig. 13). Vehoff and Rothe [5] also found {1 0 0} ⟨1 1 0⟩ fractures for HAC in ⟨1 0 0⟩ nickel single crystals.

For specimen orientations such that {1 0 0} planes were at large angles ($> \simeq 30°$) to the specimen axis, fracture surfaces were highly stepped with adjacent areas often at quite large angles to each other. Some areas exhibited approximate orthogonal networks of slip lines indicating near-{1 0 0} fracture planes but angles between slip lines in other areas showed that local deviations of up to 25° from {1 0 0} planes occurred. In some areas, there were coarse, closely spaced slip bands on fracture surfaces (Fig. 7b) and such slip, which probably occurred behind the crack tip, would produce a significant rotation of the general fracture plane towards a {1 1 1} plane.

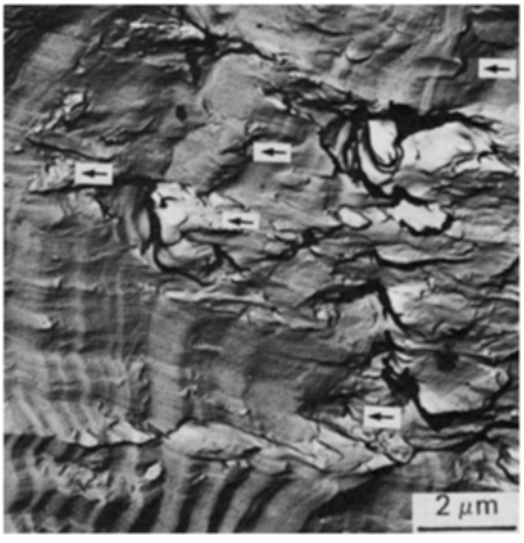


*Figure 9* TEM of fracture surface of nickel single crystal produced in hydrogen showing numerous small, shallow dimples (arrowed) and slip lines.

Kamdar [3] reported a {1 1 3} fracture plane (25° from {1 0 0}) for HAC in near-⟨1 1 1⟩ orientation specimens. Examination of these specimens and his specimens tested in mercury showed that the fractures were stepped with different areas tilted with respect to each other, as discussed above. Thus, the {1 1 3} fracture plane reported by Kamdar probably represents the approximate average fracture plane.

Eastman *et al.* [2, 13] reported a {1 1 1} fracture plane for HAC of bulk specimens with a ⟨2 2 1⟩ specimen axis. HAC in thin foils observed by high-voltage TEM also occurred on {1 1 1} planes. The occurrence of {1 1 1} fractures in thin foils is not surprising since fracture occurs under plane-stress conditions but the reason why {1 1 1} fracture planes were observed in the bulk ⟨2 2 1⟩ specimens but have not been observed in the present and other studies is not understood.

## 4. Discussion

### 4.1. Material–environment interactions

#### *4.1.1. Liquid-metal environments*

The mutual solubilities of nickel with mercury, lithium and sodium at the respective test temperatures are very small [22, 23] and, hence, reactions other than adsorption probably do not have time to occur during rapid cracking. This reasoning is generally accepted and many cases of LME have been attributed to adsorption in the past [17, 18]. Furthermore, pre-exposure of many metals to liquid-metal environments to allow time for diffusion or compound formation to occur does not produce embrittlement during subsequent testing in inert environments. There are, however, exceptions, e.g. Al–Ga [24], Ni–Bi [25], where LME is associated with diffusion of embrittling atoms into specimens along grain boundaries.

For adsorption-induced LME, it is not understood why some liquid metals are embrittling while others are apparently not embrittling. Various suggestions have been made, e.g. embrittlement couples should have low mutual solubilities, should not form high-melting point compounds, and should have small differences in electronegativity [17, 18]. For embrittlement of nickel by mercury, lithium and sodium, the first two conditions are satisfied but differences in (Pauling) electronegativity do not appear to be important. (Electronegativities of nickel, mercury, lithium and sodium are 1.8, 1.9, 1.0 and 0.9, respectively.) There does not appear to be any data on the mutual solubilities of nickel in potassium, rubidium and caesium, and it is not clear why these alkali metals do not also cause embrittlement. It is also not understood why lithium is a more potent embrittler than sodium or mercury. Presumably, differences in adsorption kinetics and the extent to which electron density (interatomic bonding) is affected by adsorption are involved. Quantum mechanical cluster calculations, as have been applied to temper embrittlement [26], could possibly throw some light on this problem.

For intercrystalline LME, the liquid-metal/solid

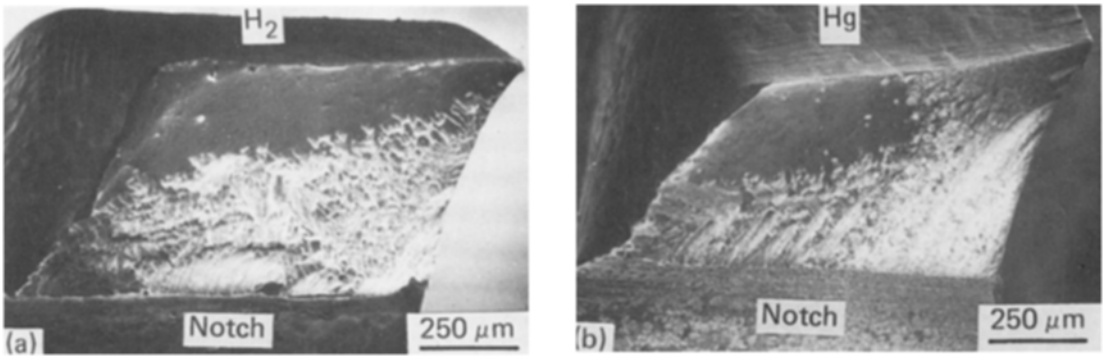


*Figure 10* SEM showing macroscopic view of fracture surfaces of Kamdar's single crystal specimens produced by tensile tests in (a) hydrogen gas (73 kPa, 20° C), and (b) liquid mercury.

metal interactions are generally complicated by the presence of segregated impurity elements at grain boundaries. Segregated impurities probably not only influence adsorption but probably also affect the strength of interatomic bonds. For example, segregation of sulphur at grain boundaries in nickel facilitates intercrystalline fracture in inert environments and exacerbates HAC [2]. On the other hand, segregation of phosphorus in nickel–copper alloys decreases the degree of embrittlement by both hydrogen and mercury [27]. However, grain-boundary segregation was not examined in the present work.

### 4.1.2. Gaseous hydrogen environments

Hydrogen molecules dissociate on clean nickel surfaces and, hence, adsorbed hydrogen atoms should be present at crack tips. Adsorbed hydrogen could then diffuse or be transported by dislocations ahead of crack tips. Thus, HAC could be due to the presence of adsorbed or dissolved hydrogen (or both). Nickel hydride forms only at hydrogen pressures greater than $\simeq 1$ GPa or during severe cathodic charging [2] and, hence, should not be involved for the present tests.

The remarkable similarities between HAC and LME suggest that adsorbed hydrogen could be responsible for HAC. Different fracture mechanisms can sometimes produce superficially similar fracture-surface appearances but, for nickel single crystals, the fine details on fracture surfaces, the fracture plane, the direction of crack growth, and the extent and distribution of slip around crack tips were the same after cracking in mercury and hydrogen. Furthermore, the appearance of fractures was somewhat different for different crystal orientations but was the same for hydrogen and mercury environments for each orientation. Thus, it is highly probable that the mechanisms of HAC and LME are the same.

The observation that HAC can occur at crack velocities as high as $\simeq 1\,\mathrm{mm\,sec^{-1}}$ also suggests that adsorbed hydrogen is responsible since rates of diffusion are too slow for hydrogen to diffuse ahead of cracks. Taking the diffusion coefficient, $D$, of hydrogen in nickel as $10^{-14}\,\mathrm{m^2\,sec^{-1}}$ [28], the diffusion distance $[\simeq 4(Dt)^{1/2}]$ for $t \simeq 10^{-6}$ sec (the time for a crack-growth increment of several atomic distances for a crack velocity $\simeq 1\,\mathrm{mm\,sec^{-1}}$) is about one atomic distance. Hydrogen could be transported rapidly by dislocations providing that dislocation velocities are below a critical value [28]. However, it is doubtful if adsorbed hydrogen would be transported into specimens during fast crack growth since dislocation velocities around crack tips are probably very high. For

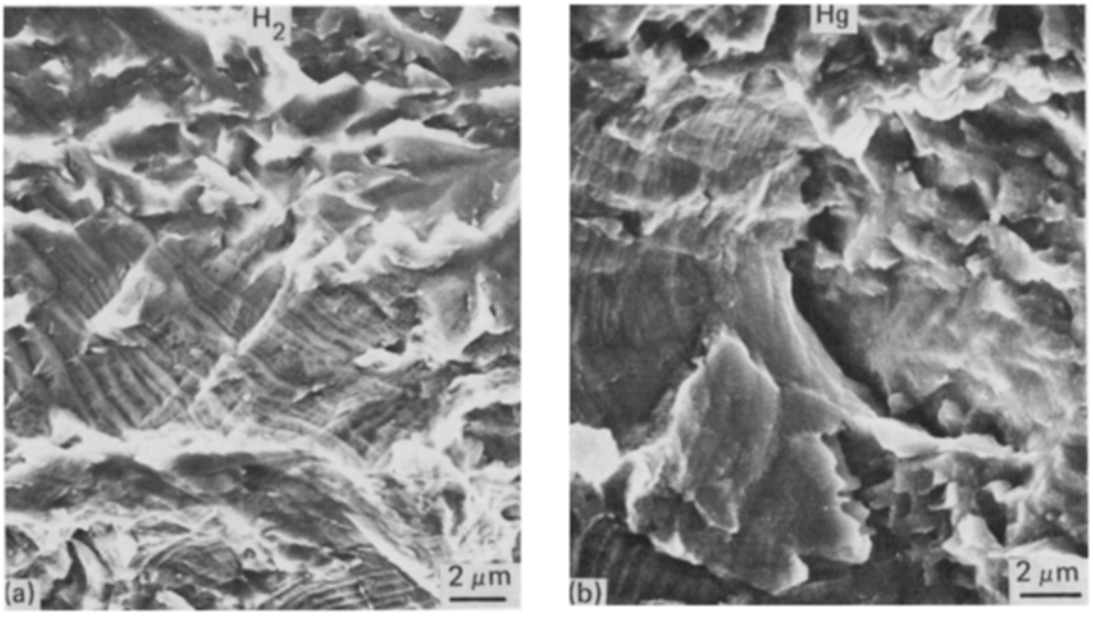


*Figure 11* SEM of fracture surfaces near notch shown in Fig. 10, at a higher magnification showing slip lines, steps, and tear ridges.

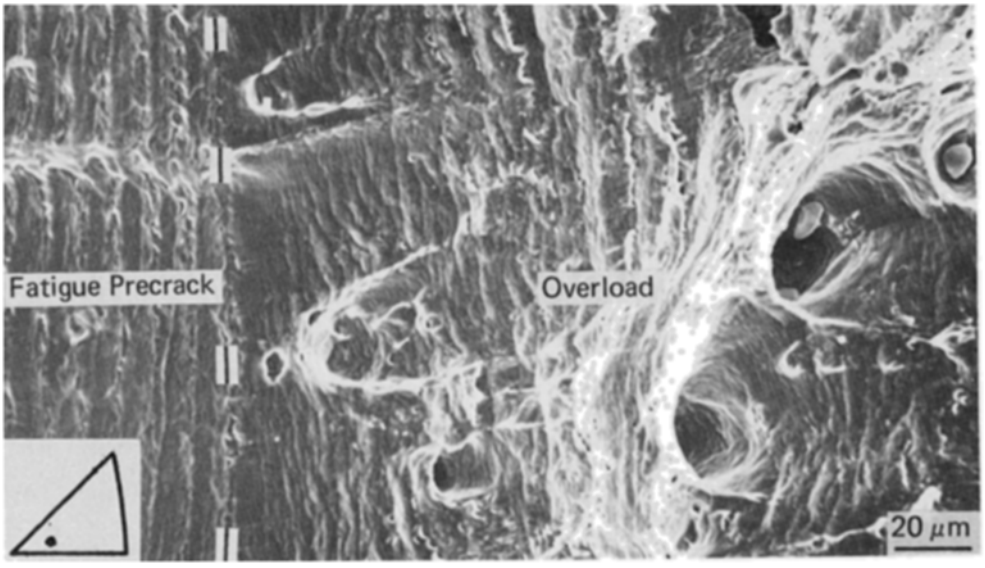


*Figure 12* SEM of fracture surface of hydrogen-charged nickel single crystal showing "ductile" striations produced by fatigue precracking, and a stretched zone and large deep dimples produced by overload at slow strain rate, i.e. no evidence of embrittlement.

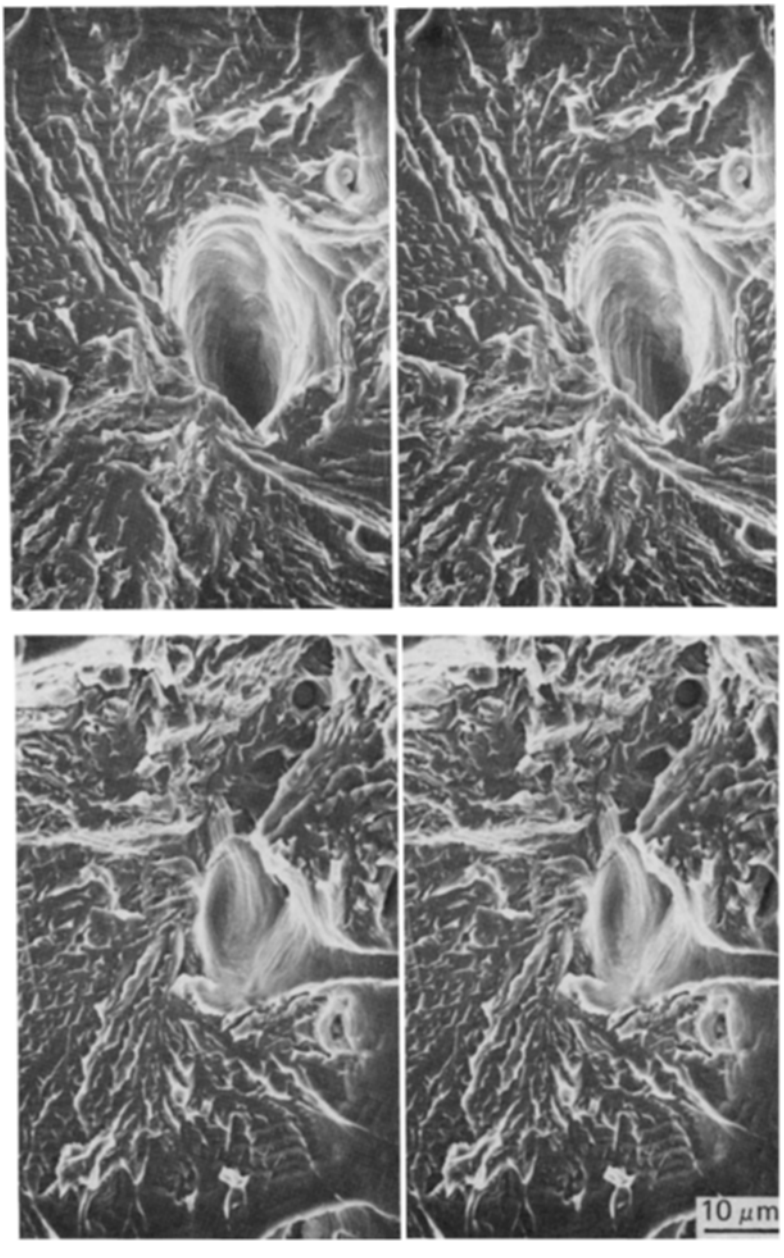


*Figure 13* SEM (stereographic pairs) of mating halves of opposite fracture surfaces for the same hydrogen-charged nickel single crystal as in Fig. 12 showing "brittle" regions around a large dimple some distance ahead of the fatigue precrack.

single crystals, even if such transport did occur, hydrogen would be transported along {1 1 1} planes inclined at $\simeq 54°$ to {1 0 0} crack planes unless hydrogen was subsequently transferred to dislocations moving towards the crack tip on other slip planes.

Kamdar [3] found that the degree of embrittlement and fracture-surface characteristics of nickel single crystals in gaseous hydrogen were not affected by the testing temperature over the range $-130$ to $+20°$ C. These observations are a further indication that adsorbed hydrogen is responsible for HAC since the rates of diffusion and the solute hydrogen concentration would vary markedly over this temperature range whereas adsorption kinetics are probably less sensitive to temperature. Furthermore, HAC probably occurs by slip (as discussed later) and the effects of dissolved hydrogen on dislocation activity are different at different temperatures [1, 2].

#### 4.1.3. Hydrogen-charged specimens

Crack growth from the tip of a fatigue crack in single crystals containing $\simeq 0.045$ at % solute hydrogen was initially ductile, even at low crack velocities when hydrogen would have time to diffuse and concentrate ahead of cracks. Other workers [7] have also found that hydrogen-charged single crystals are completely ductile. These observations, taken with the other observations discussed above, show that there can be little doubt that adsorbed hydrogen rather than dissolved hydrogen is responsible for HAC.

The areas of "brittle" cracking around some large dimples some distance ahead of fatigue pre-cracks in hydrogen-charged single crystals can be readily explained in terms of adsorbed hydrogen. Thus, large voids probably contain gaseous hydrogen, with adsorbed hydrogen at void tips, since solute hydrogen probably diffuses or is transported by dislocations to voids during slow crack growth. Only particularly large dimples were surrounded by "brittle" areas suggesting that voids must reach a certain size before sufficient hydrogen accumulates within them to produce HAC. Work-hardening around voids probably also increases the material's susceptibility to HAC.

For hydrogen-charged polycrystals, the areas of cleavage-like cracking and "brittle" intercrystalline cracking are probably also associated with diffusion of hydrogen to, and adsorption at, the tips of internal voids/cracks. However, for intercrystalline HAC there may be sufficient atomic hydrogen trapped at grain boundaries that interatomic bonds at advancing crack tips are always associated with hydrogen. This is assuming that the fracture path exactly follows the grain boundary and not a path close to the boundary as some recent observations suggest [29].

### 4.2. Possible mechanisms of adsorption-assisted cracking

#### 4.2.1. Decohesion at crack tips

The traditional view is that adsorption facilitates tensile separation of atoms ("decohesion") at crack tips but does not directly influence dislocation activity around cracks [30, 31]. Thus, it is envisaged that atomically brittle fracture can occur in normally ductile materials because adsorption lowers the stress required for decohesion to a level below that required for slip on planes intersecting crack tips.

Decohesion should produce atomically sharp crack tips and essentially flat fracture surfaces. Some slip may accompany decohesion providing strains are very low and dislocations do not generally intersect crack tips. Such characteristics are observed for cleavage fracture of intrinsically brittle materials such as zinc single crystals. Furthermore, the stress required for cleavage in zinc is $\simeq 40\%$ lower in liquid mercury than in air showing that adsorption can facilitate decohesion [32]. However, the characteristics of cleavage-like fractures produced by HAC and LME in nickel are entirely different from those produced by cleavage in zinc and slip processes are clearly involved during HAC and LME in nickel.

#### 4.2.2. Decohesion plus slip at crack tips

Crack growth involving repeated sequences of adsorption-induced decohesion and then alternate-slip on planes intersecting crack tips could possibly produce cleavage-like fractures associated with considerable slip. Alternate slip at crack tips could be necessary to open the crack to allow subsequent adsorption and decohesion [33]. However, the observations of LME in zinc single crystals mentioned above suggest that adsorption can keep up with rapidly growing atomically sharp crack tips. Furthermore, an analysis [34] has shown that equal amounts of slip on either side of the crack, as observed, should not favour subsequent decohesion. Thus, there is not an obvious reason why sequences of slip and decohesion should occur at crack tips.

It has also been suggested [35] that atomically sharp crack tips produced by decohesion could be broadened on a macroscopic scale by inhomogeneous slip behind crack tips. Coarse slip bands are observed on cleavage-like and intercrystalline fractures in nickel suggesting that cracks are broadened by such an effect. However, crack tips in nickel are unlikely to be atomically sharp since such high strains are observed around cracks, crack fronts are parallel to the line of intersection of slip planes with crack planes, and dimples are observed on fracture surfaces. In other words, the evidence suggests that HAC and LME in nickel occurs entirely by localized plastic flow and that decohesion is not involved.

#### 4.2.3. Localized slip at crack tips

There is now growing recognition [4, 18, 26, 36] that adsorption-induced weakening of interatomic bonds at crack tips must not only reduce the stress required for tensile separation of atoms but must also reduce the stress necessary for shear movement of atoms (dislocation nucleation) at crack tips. The preliminary work on HAC and LME in nickel [4], observations of HAC and LME in other intrinsically ductile materials [37–39], and the present observations are all consistent with the idea that adsorption facilitates nucleation of dislocations at crack tips. Specifically, it has been proposed [4, 37–39] that ingress of dislocations

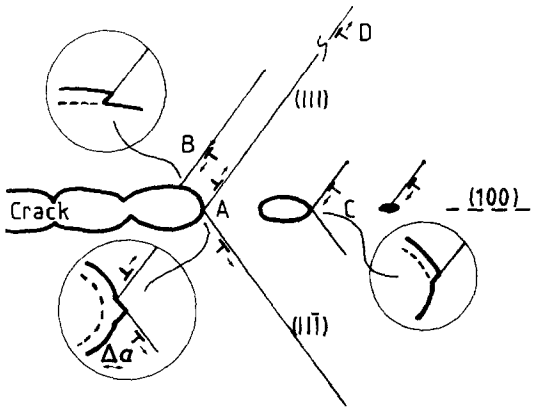


*Figure 14* Schematic diagram illustrating dislocation activity around crack tips during ductile and "brittle" crack growth: (A) dislocations producing crack advance, e.g. those nucleated at the crack tip, (B) dislocations producing blunting, e.g. those egressing behind the crack tip, (C) dislocations involved in nucleation and growth of voids, (D) dislocations in plastic zone away from crack-tip region. For HAC/LME, adsorption facilitates dislocation nucleation at crack tips so that A predominates. For ductile fracture, dislocation nucleation at crack tips is difficult and, hence, other dislocation activity predominates.

from crack tips produces crack growth and thereby promotes the coalescence of cracks with voids ahead of cracks (Fig. 14). The growth of voids is not directly influenced by adsorption but is necessary to re-sharpen crack tips so that crack growth is macroscopically brittle.

A basic premise of the proposed adsorption-induced dislocation–nucleation mechanism of HAC/LME is that dislocation nucleation in inert or air environments is difficult so that ductile crack growth occurs predominantly by egress of dislocations at crack tips. Only a small proportion of dislocations nucleated from near-crack-tip sources would egress exactly at crack tips to produce crack growth – most dislocations would either egress behind the crack tip or remain ahead of cracks to produce blunting and large strains at crack tips. Facilitating dislocation nucleation from crack tips can then increase the proportion of dislocations producing crack advance and thereby reduce the strains necessary for crack growth, i.e. produce embrittlement.

Crack growth by adsorption-induced ingress of dislocations from crack tips involves approximately equal amounts of slip on two {1 1 1} slip planes intersecting crack tips since, if more dislocations were emitted on one side of the crack than the other, then a larger back stress on subsequent dislocations emitted from the crack would build up on the more active side and inhibit further emission. Thus, the macroscopic fracture plane bisects the angle between the two slip planes and crack fronts are parallel to the line of intersection of slip planes with crack planes, i.e. {1 0 0} fractures with ⟨1 1 0⟩ growth directions are produced. Deviations from {1 0 0} fracture planes, which occur especially when {1 0 0} planes are steeply inclined to the stress axis, probably arise because slip planes on one side of the crack are then so much more highly stressed than those on the other side that slip occurs preferentially on one side of the crack.

### 4.3. Effects of adsorption on surfaces

There are no direct experimental techniques for determining the strength of interatomic bonds at crack tips but there are some interesting observations and theoretical calculations which are possibly relevant to understanding HAC and LME.

Observations of surfaces by low-energy electron diffraction (LEED) [40,41] and other techniques have shown that, for some clean metal surfaces, there are significant changes of lattice parameter normal to the surface for the first one or two atomic layers. LEED observations show that adsorption of oxygen on many metal surfaces produces disruption of the surface lattice with incorporation of oxygen atoms into the top-most layer of substrate atoms, i.e. an incipient oxide film is formed [40]. Thus, crack growth in both air/oxygen and inert environments is ductile possibly because oxide films and clean-surface perturbations, respectively, inhibit dislocation nucleation [42] so that crack growth occurs by egress of dislocations at crack tips. On the other hand, weak chemisorption of some species can remove or reduce the clean-surface lattice perturbations or, occasionally, produce a reconstruction of the surface [40]. Such effects could possibly be involved in facilitating the nucleation of dislocations.

Atomistic calculations of fracture in the presence of hydrogen using an "embedded atom method" [43, 44] suggest that hydrogen can weaken interatomic bonds so that decohesion or dislocation nucleation at crack tips occurs at lower stresses than in inert environments. Quantum mechanical cluster calculations have also shown that the presence of impurity atoms can decrease the electron density (and possibly the strength of interatomic bonds) between atoms [26]. Cluster calculations for adsorbed hydrogen on beryllium suggested that high tensile stresses could be induced in the surface layers by adsorption thereby facilitating dislocation nucleation [45]. Computer modelling of crack-tip behaviour [46, 47] also suggests that dislocation nucleation is sensitive to changes of lattice parameter in the first few surface atomic layers.

Direct experimental evidence that adsorption influences dislocation activity is difficult to obtain since the mechanical properties of specimens with small surface/volume ratios would not be expected to be sensitive to adsorption. Observed effects of environment on plasticity in thin foils could be due to adsorption but other effects cannot be ruled out. For example, observations [13] that dislocation activity in nickel foils is increased when gaseous hydrogen is introduced could be due to adsorbed or solute hydrogen or possibly reduction of oxide films. Field-ion microscopy observations [48] of iron surfaces in hydrogen environments suggested that adsorbed hydrogen could facilitate nucleation of dislocations but again other effects could be involved.

Video-tape recordings of crack growth in thin foils of a number of materials including nickel using HVEM [49, 50] directly show that crack growth occurs by plastic flow and sometimes involves formation of small voids ahead of cracks in both inert and hydrogen environments. Furthermore, the stress necessary to cause the plasticity which leads to fracture is reduced in hydrogen and the plasticity is more

localized near the crack tip in hydrogen than in inert environments. These observations, which are entirely consistent with the present observations in bulk specimens, were explained in terms of a localized softening of material around crack tips due to interactions of dislocations with solute hydrogen. However, softening is only observed under certain conditions whereas HAC occurs under many conditions, including those where serrated yielding and hardening have been observed. These and the present observations suggest that HAC can best be explained on the basis that adsorbed hydrogen facilitates the nucleation of dislocations at crack tips.

## 5. Conclusions

1. Hydrogen-assisted cracking in nickel single crystals is caused by adsorbed hydrogen rather than by dissolved hydrogen. This conclusion is based mainly on observations that
   (a) the characteristics of HAC were remarkably similar to those of adsorption-induced LME.
   (b) HAC could occur at crack velocities as high as $\simeq 1\,\mathrm{mm\,sec^{-1}}$, and
   (c) solute hydrogen introduced by hydrogen-charging does not produce embrittlement.

2. Hydrogen-assisted cracking in nickel single crystals occurs by localized plastic flow rather than by decohesion. This conclusion is based on observations that
   (a) crack growth was associated with large strains (large crack-opening angles) with extensive slip on $\{1\,1\,1\}$ planes intersecting near-$\{1\,0\,0\}$ cracks,
   (b) crack fronts were parallel to the line of intersection of slip planes with crack planes, and
   (c) fracture surfaces were covered with dimples and tear ridges.

3. Hydrogen-assisted intercrystalline cracking in nickel polycrystals is also similar to adsorption-induced intercrystalline LME and is associated with large strains and, hence, mechanisms of intercrystalline and transcrystalline fracture are probably similar.

4. It is concluded that adsorption facilitates nucleation of dislocations at crack tips, and thereby promotes coalescence of cracks with voids, whereas in inert environments crack growth occurs predominantly by egress of dislocations at crack tips.

## Acknowledgements

The author would like to thank P. Trevena, AERE, Harwell for assistance with the tests in liquid alkali metals, and M. H. Kamdar for supplying some high-purity nickel single crystals.

## References

1. B. A. WILCOX and G. C. SMITH, *Acta Metall.* **13** (1965) 331.
2. J. EASTMAN, T. MATSUMOTO, N. NARITA, F. HEUBAUM and H. K. BIRNBAUM, in "Hydrogen Effects in Metals", edited by I. M. Bernstein and A. W. Thompson (Metallurgical Society AIME, Warrendale, Pa. 1981) p. 397.
3. M. H. KAMDAR, in Second International Congress on Hydrogen in Metals (Pergamon Press, Oxford, 1977) 3D12.
4. S. P. LYNCH, *Scripta Metall.* **13** (1979) 1051.
5. H. VEHOFF and W. ROTHE, *Acta Metall.* **31** (1983) 1781.
6. R. H. JONES, S. M. BRUEMMER, M. T. THOMAS and D. R. BAER, *Metall. Trans.* **14A** (1983) 1729.
7. A. H. WINDLE and G. C. SMITH, *Met. Sci. J.* **4** (1970) 136.
8. B. A. WILCOX and G. C. SMITH, *Acta Metall.* **12** (1964) 371.
9. A. H. WINDLE and G. C. SMITH, *Met. Sci. J.* **2** (1968) 187.
10. R. M. LATANISION and H. OPPERHAUSER Jr, *Metall. Trans.* **5** (1974) 483.
11. E. LUNARSKA and J. FLIS, *Scripta Metall.* **18** (1984) 889.
12. T. MATSUMOTO, J. EASTMAN and H. K. BIRNBAUM, *ibid.* **15** (1981) 1033.
13. J. EASTMAN, F. HEUBAUM, T. MATSUMOTO and H. K. BIRNBAUM, *Acta Metall.* **30** (1982) 1579.
14. I. M. ROBERTSON and H. K. BIRNBAUM, *Scripta Metall.* **18** (1984) 269.
15. W. A. McINTEER, A. W. THOMPSON and I. M. BERNSTEIN, *Acta Metall.* **28** (1980) 887.
16. M. R. LOUTHAN Jr, G. R. CASKEY Jr, J. A. DONOVAN and D. E. RAWL Jr, *Mater. Sci. Eng.* **10** (1972) 357.
17. M. H. KAMDAR, *Prog. Mater. Sci.* **15** (1973) 289.
18. N. S. STOLOFF, in "Atomistics of Fracture", edited by R. M. Latanision and J. R. Pickens (Plenum Press, New York, 1983) p. 921.
19. N. M. PARIKH, in "Environment Sensitive Mechanical Behaviour", edited by A. R. C. Westwood and N. S. Stoloff (Gordon and Breach, New York, 1966) p. 563.
20. W. T. GRUBB, in "Embrittlement by Liquid and Solid Metals", edited by M. H. Kamdar (Metallurgical Society AIME, Warrendale, Pa., 1984) p. 473.
21. M. G. NICHOLAS and P. TREVENA, AERE Report 10559, Harwell, June 1982.
22. M. HANSEN, "Constitution of Binary Alloys", 2nd edn, (McGraw-Hill, New York, 1958) p. 828.
23. R. P. ELLIOTT, "Constitution of Binary Alloys" 1st Supplement (McGraw-Hill, New York, 1965) pp. 584, 648.
24. C. ROQUES-CARMES, M. AUCOUTURIER and P. LACOMBE, *Met. Sci.* 7 (1973) 128.
25. G. H. BISHOP, *Trans. Met. Soc. AIME* **242** (1968) 1343.
26. M. E. EBERHART, K. H. JOHNSON and R. M. LATANISION, *Acta Metall.* **32** (1984) 955.
27. A. W. FUNKELBUSCH, L. A. HELDT and D. F. STEIN, in "Embrittlement by Liquid and Solid Metals", edited by M. H. Kamdar (Metallurgical Society AIME, Warrendale, Pa., 1984) p. 124.
28. J. K. TIEN, S. V. NAIR and R. R. JENSEN, in "Hydrogen Effects in Metals", edited by I. M. Bernstein and A. W. Thompson (Metallurgical Society AIME, Warrendale, 1981) p. 37.
29. I. M. ROBERTSON, T. TABATA, W. WEI, F. HEUBAUM and H. K. BIRNBAUM, *Scripta Metall.* **18** (1984) 841.
30. N. S. STOLOFF and T. L. JOHNSTON, *Acta Metall.* **11** (1963) 251.
31. A. R. C. WESTWOOD, C. M. PREECE and M. H. KAMDAR, *Trans. ASM* **60** (1967) 723.
32. A. R. C. WESTWOOD and M. H. KAMDAR, *Phil. Mag.* **8** (1963) 804.
33. L. B. VOGELSANG and J. SCHIJVE, *Fat. Enging. Mater. Struct.* **3** (1980) 85.
34. J. E. SINCLAIR and M. W. FINNIS, in "Atomistics of Fracture", edited by R. M. Latanision and J. R. Pickens (Plenum Press, New York, 1981) p. 1047.
35. R. THOMSON, *J. Mater. Sci.* **13** (1978) 128.
36. R. A. ORIANI, *Scripta Metall.* **18** (1984) 265.
37. S. P. LYNCH, *Acta Metall.* **29** (1981) 325.
38. *Idem, ibid.* **32** (1984) 79.
39. *Idem, Scripta Metall.* **18** (1984) 509.
40. G. A. SOMORJAI and M. A. VAN HOVE, in "Structure and Bonding", edited by J. D. Dunitz *et al.* (Springer, Berlin, 1979) Vol. 38.

41. R. FEIDENHANS'L, J. E. SØRENSEN and I. STENSGAARD, *Surf. Sci.* **134** (1983) 329.
42. R. L. FLEISCHER, *Acta Metall.* **8** (1960) 598.
43. M. S. DAW and M. I. BASKES, *Phys. Rev. B* **29** (1984) 6443.
44. *Idem,* unpublished results, Sandia National Laboratories, Livermore, California, 1984.
45. B. N. COX and C. W. BAUSCHLICHER Jr, *Surf. Sci.* **102** (1981) 295.
46. A. PASKIN, K. SIERADZKI, D. K. SOM and G. J. DIENES, *Acta Metall.* **31** (1983) 1253.
47. A. PASKIN, B. MASSOUMZADEH, K. SIERADZKI and G. J. DIENES, *Scripta Metall.* **18** (1984) 1135.
48. J. A. CLUM, *ibid.* **9** (1975) 51.
49. T. TABATA and H. K. BIRNBAUM, *ibid.* **18** (1984) 231.
50. I. M. ROBERTSON, unpublished results, University of Illinois, 1984.

*Received 11 February*
*and accepted 22 April 1985*